Integration of Edge-Emitting Quantum Dot Lasers With Different Waveguide Platforms Using Micro-Transfer Printing

Ali Uzun, Fatih Bilge Atar, Simone Iadanza, Ruggero Loi, Jing Zhang, Gunther Roelkens, *Senior Member, IEEE*, Igor Krestnikov, Johanna Rimböck, Liam O'Faolain, *Member, IEEE*, and Brian Corbett

(Invited Paper)

***Abstract*—O-band InAs/GaAs Quantum Dot edge-emitting lasers are integrated onto a number of waveguiding platforms using micro-transfer printing. These are deep recesses in 220 nm Si, 3 μm Si and 300 nm SiN waveguide circuits. The processing technology to achieve release and high-yield accurate transfer of laser coupons up to 2.4 mm long and <5 μm thick onto the target substrates is described. At 85 mA, waveguide coupled powers of 1.0 mW and 0.95 mW are measured after out-coupling from the 220 nm SOI and 300 nm SiN waveguides, respectively while 1.7 mW total power was measured from the 3 μm SOI waveguide.**

***Index Terms*—Silicon photonics, heterogeneous integration, data centers, Si waveguide, SiN waveguide, semiconductor laser.**

I. Introduction

PHOTONIC integrated circuits (PICs) allow complex optical systems to be miniaturized to chip scale opening new applications as well as reducing energy consumption. They can be manufactured in foundries at decreasing cost with volume as has been so successful for electronic circuits. Currently, the primary applications are in transceivers for the data communications industry [1], but the technology is increasingly being applied to signal processing [2], 5G, LiDAR, metrology, sensing, neuromorphic & machine learning [3] with future opportunities in high volume consumer applications. PICs are being developed on a number of different material platforms. The InP-based platform provides very high functionality [4], though the integration is complex and proprietary. The main industry focus is on the silicon-on-insulator (SOI) platform as silicon (Si) provides an ideal waveguide for near-infrared wavelengths due to its large index contrast with the surrounding silicon dioxide (SiO_2). Scalability is enabled through the use of 200 and 300 mm diameter wafers on the established complementary metal–oxide–semiconductor (CMOS) foundry process technology, which is suited for many optical properties, especially smooth sidewalls for low-loss waveguides. The Si waveguiding layer thickness ranges from 220 nm to 3 μm. PICs covering an expanded wavelength range are enabled by the silicon nitride (SiN) platform which benefits from ultra-low loss waveguides [5]. Lithium Niobate on insulator (LNOI) is emerging [6] as an interesting alternative platform due to its strong non-linear / electro-optic properties.

The Si, Si_3N_4 and LNOI platforms lack an integrated optical amplifier which can only be provided by direct bandgap III-V materials. To address this, the optical power can be delivered from an external source and coupled to the waveguide using surface gratings or by edge-coupling. The spectral bandwidth of gratings is limited and requires fiber attachment while edge-coupling requires the preparation of end facets after the wafer manufacture. Thus, a fully integrated solution is desired. One approach is the flip-chip mounting of separately manufactured lasers with respect to the edge of the waveguides. This can be performed in a hybrid manner to the edge of the chip [7] or, preferably, in an integrated manner to internally etched facets of the waveguide. This requires precise submicron alignment, which can be achieved through control of all the relevant dimensions and use of fiducials during the flip-chip mounting [8]. The throughput is however low. So far, evanescent coupling has proven to be the most successful approach and is enabled by

Manuscript received 24 August 2022; revised 29 November 2022; accepted 29 November 2022. Date of publication 10 February 2023; date of current version 20 February 2023. This work was supported in part by the CALADAN Project under Grant Agreement 825453, in part by Science Foundation Ireland through IPIC under Grant 12/RC/2276_P2, and in part by the Disruptive Technologies Innovation Fund under Grant DT 2019 0080. (*Corresponding author: Ali Uzun.*)

Ali Uzun, Fatih Bilge Atar, and Brian Corbett are with the Tyndall National Institute, University College Cork, T12 R5CP Cork, Ireland (e-mail: ali.uzun@tyndall.ie; fatih.atar@tyndall.ie; brian.corbett@tyndall.ie).

Simone Iadanza and Liam O'Faolain are with the Munster Technological University, T12 P928 Cork, Ireland (e-mail: simone.iadanza@mtu.ie; william.whelan-curtin@mtu.ie).

Ruggero Loi is with the X-Celeprint Limited, T12 R5CP Cork, Ireland (e-mail: rloi@x-celeprint.com).

Jing Zhang and Gunther Roelkens are with the Photonics Research Group, INTEC, Ghent University—imec, 9052 Ghent, Belgium (e-mail: jingzhan.zhang@ugent.be; gunther.roelkens@ugent.be).

Igor Krestnikov is with the Innolume GmbH, 44263 Dortmund, Germany (e-mail: igor.krestnikov@innolume.com).

Johanna Rimböck is with the EV Group E.Thallner GmbH, 4782 Florian am Inn, Austria (e-mail: j.rimboeck@evgroup.com).

Color versions of one or more figures in this article are available at https://doi.org/10.1109/JSTQE.2023.3243943.

Digital Object Identifier 10.1109/JSTQE.2023.3243943

This work is licensed under a Creative Commons Attribution 4.0 License. For more information, see https://creativecommons.org/licenses/by/4.0/

wafer bonding of the III-V gain material to the Si waveguide platform, substrate removal and subsequent device manufacture [9]. Limitations are the inability to pre-test devices, the cost of the III-V materials and the proximity that different components can be placed at.

Micro-transfer printing (MTP) [10] is emerging as an interesting alternative integration technology for active and passive devices in silicon photonics. Releasable coupons are prepared in a grid and then, arrays of devices are selectively transferred from their native III-V substrate to target waveguide wafers in a highly parallel manner using a structured polydimethylsiloxane (PDMS) stamp [11]. The coupons comprise simply the gain material itself or fully formed devices, thus enabling fabrication of optimized components in either the Si or III-V foundry [12]. The coupons are bonded to the target wafer either directly through van der Waals forces or by using a thin adhesive layer. This enables light coupling from the III-V waveguide to the SOI waveguide through engineered evanescent coupling. The approach makes very efficient use of the III-V source while coupons of different materials can be placed adjacent to each other. A particular advantage of MTP over wafer bonding is the ability to print the coupons into trenches on non-planar wafers and thus achieve edge-coupling and is the subject of this paper. MTP has been previously applied in silicon photonics with demonstrated evanescently coupled semiconductor optical amplifiers SOAs [13], single frequency lasers [14], quantum sources [15], ring resonators [16], edge-coupled lasers [17], [18], grating coupled photodiodes [19], [20].

In this paper, we demonstrate heterogeneous integration and edge-coupling of quantum dot (QD) lasers emitting around 1300 nm (O-band) using MTP to different waveguiding platforms namely 220 nm Si, 3 μm Si and 300 nm SiN. Section II describes the strategy for light coupling to the different waveguide platforms, Section III, the laser fabrication and coupon preparation for high-yield MTP where etched-facet ridge waveguide QD lasers with 1.5 mm long cavities show threshold currents of 17 mA and output powers above 20 mW at 120 mA injection current. Section IV shows the experimental results where, at 85 mA drive current waveguide coupled powers of 1 mW and 0.95 mW are obtained after propagation through 220 nm Si and 300 nm SiN waveguides, respectively. 1.7 mW total power is measured from the 3 μm Si waveguide at 85 mA. Section V concludes the paper.

II. Integration Platforms

We consider a number of different waveguiding platforms for the integration of edge-coupled QD lasers using MTP. Fig. 1 depicts the studied configurations utilising (a) 220 nm SOI, (b) 3 μm SOI, and (c) 300 nm SiN. The advantages of edge-coupling are the low wavelength and polarization dependence and only a single interface between the waveguides. The coupling efficiency is dependent on the mismatch in the mode sizes of the laser and passive waveguide, the refractive index in the gap between the laser and waveguide along with any misplacement in lateral, vertical and longitudinal dimensions.

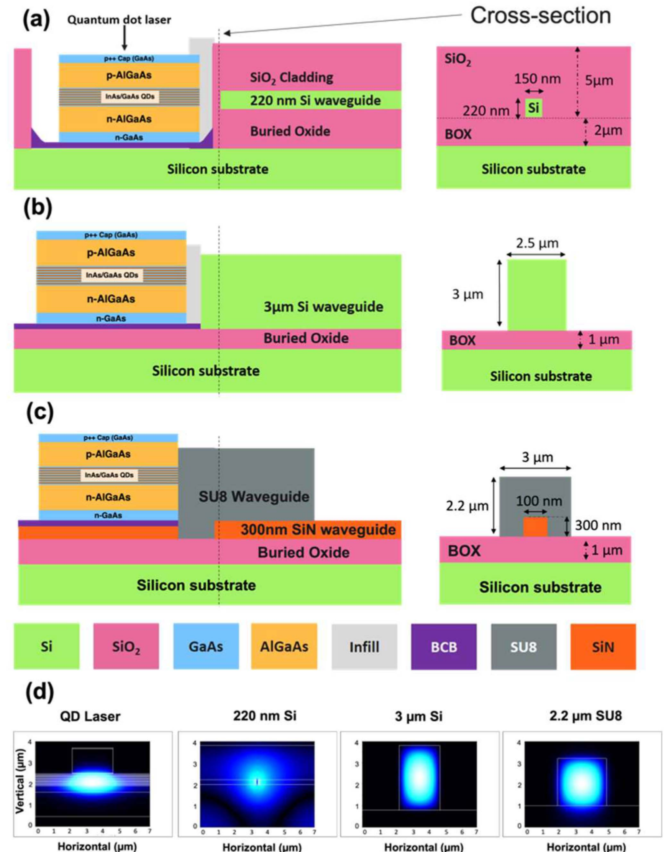

Fig. 1. Edge-coupling configurations for different waveguide platforms. (a) QD laser transferred inside a deep recess where light is coupled to 220 nm Si waveguide. Cross-section of thin Si waveguide with 2 μm BOX layer and 5 μm top SiO_2 cladding (right). (b) Transferred laser next to a 3 μm Si waveguide on 70 nm BCB layer on the BOX layer and cross-section of 2.5 μm wide waveguide (right). (c) Laser printed on remaining SiN layer and coupled to SiN waveguide via SU-8 down-coupler and waveguide cross-section at the start of SiN (right). (d) Simulated electric field profiles of the fundamental TE mode in the QD laser and the respective waveguides.

The first platform is the imec 220 nm silicon photonics platform with a 2 μm buried oxide (BOX) and a 5 μm thick SiO_2 over-cladding. Trenches to facilitate edge-coupling have been introduced to this platform as schematically shown in Fig. 1(a). These are 7 μm deep and accurately stop at the interface to the Si handle wafer surface. The trenches are 120 μm wide and 2.5 mm long to accommodate the QD lasers. The receiving Si waveguides have a single inverse tapered tip which expands the mode reducing its effective index close to that of SiO_2 for improved alignment tolerance and better mode-size matching. One particular challenge for this design is the tight vertical alignment tolerance due to strong vertical mode confinement typical of QD lasers. This requires matched calibrated n-cladding thickness in the laser epitaxial layer for achieving vertical alignment between the generating and receiving waveguides. It is also possible to tailor the vertical alignment by adjusting the etch depth into the SOI substrate and by the use of a thin adhesive layer. An edge-coupling efficiency of 65% (−2 dB) is simulated with a lateral and vertical alignment of <1.3 μm and <0.7 μm for 3 dB excess loss, respectively [Fig. 2(a)]. In addition, the longitudinal

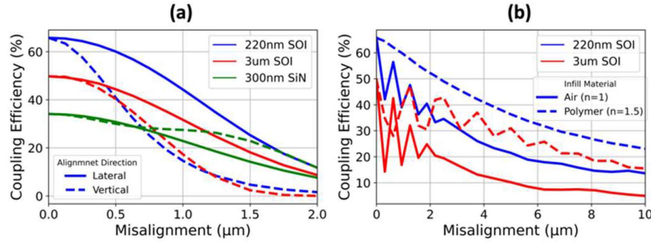

Fig. 2. Simulated coupling efficiencies as a function misalignment in lateral, vertical and longitudinal directions for fundamental TE mode transmission from a laser (2.5 μm ridge) to 220 nm SOI, 3 μm SOI and 300 nm SiN waveguide. (a) Horizontal (continuous line) and vertical (dashed line) misalignment, and (b) Longitudinal misalignment with air-gap (continuous line) or in-filled with polymer of n = 1.5 (dashed line).

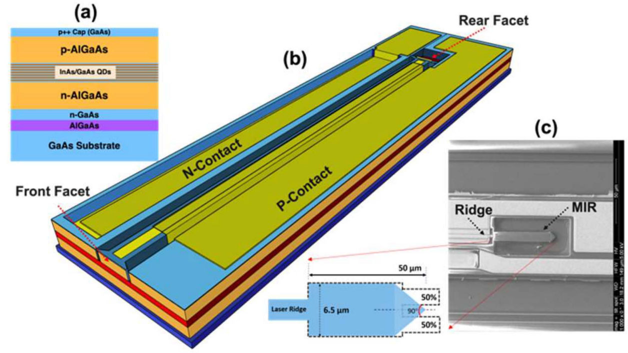

Fig. 3. (a) GaAs QD laser epitaxial structure grown by Innolume GmbH, (b) Laser coupon schematic showing the metal top contacts, ridge waveguide and mirror. (c) SEM image of a MIR mirror (6.5 μm wide and 50 μm long) and the inset shows a schematic of the MIR derivation from 1x2 MMI.

spacing between the laser facet and receiving Si waveguide has a 3 dB excess loss coupling tolerance of 5.5 μm considering an in-fill refractive index of 1.5 as given in Fig. 2(b). The in-fill also reduces the impact of an undesired Fabry-Perot cavity. This strategy provides an excellent thermal sink for the lasers as they sit directly on high thermal conductivity Si or on a thin adhesive (<100 nm) in comparison to the evanescent coupling approach where the laser is placed above the buried oxide. Initial results were described in [21].

The second platform is 3 μm thick SOI with a 1 μm BOX layer. This platform configuration has shown low propagation loss, low polarization dependency and ability to tolerate high power [22] as compared to the submicron Si waveguide. For this paper, fully etched straight waveguides, 2.5 μm wide, are fabricated in a single step process. The QD laser is transfer-printed next to the end facet as depicted in Fig. 1(b). The coupling efficiency from a laser with 2.5 μm wide ridge into a 2.5 μm wide deep-etched Si waveguide is simulated to be 50%. A similar 3 dB excess loss lateral (<1.3 μm) and vertical (<0.75 μm) positioning tolerance is simulated with 3 μm SOI for 2.5 μm transmitting and receiving waveguide as shown in Fig. 2(a). Vertical alignment could be achieved by adjusting the etch depth in BOX layer without any changes in laser epitaxial structure. This design would give a relatively poorer thermal conductivity when the laser is integrated directly on the BOX layer as it has a much lower thermal conductivity than Si. However, the laser could be transferred on Si with or without an adhesive layer after removal of the BOX layer by a proper design of epitaxial stack. There is a need for an in-fill between the laser and waveguide since an air gap introduces strong reflections as the mode index for both the laser and the Si is high. A 3 dB excess loss longitudinal tolerance of 6 μm is achievable with in-fill material (n $\sim$1.5) as given in Fig. 2(b).

The third platform is 300 nm thick SiN deposited on a 1 μm BOX layer on a Si substrate. The 1 μm wide waveguides are defined by dry etching 2 μm wide trenches around them. In contrast to the first two edge-couplers, this design employs a SU-8 polymer spot size converter (SSC) [23] where the light is first edge-coupled from the laser into the SU-8 waveguide and then evanescently coupled from the SU-8 waveguide to the underlying SiN waveguide by tapering down and up both SU-8 and SiN waveguides, respectively. The simulated coupling efficiency in this configuration is 35% as given in Fig. 2(a). The transmission from laser to SU-8 waveguide (35%) limits the overall coupling, with the simulated coupling from SU-8 SSC to underlying SiN waveguide being >95%. The 3 dB excess loss positioning tolerance in the lateral and vertical directions are 1.25 μm and 1.75 μm, respectively. The alignment in lateral and vertical direction can be tailored by adjusting the width and thickness of SU-8 waveguide.

III. Laser Fabrication for MTP

A. Quantum Dot Laser

Optical communication in data centres has converged on the use of signals in the O-band (1300 nm range). Lasers in this wavelength range can be obtained by the use of QD emitters based on GaAs technology. This provides several scaling and practical advantages. GaAs wafer technology is more mature compared to that of InP especially with the availability of high-quality, large diameter wafers. AlGaAs layers have high bandgaps that enable enhanced mode overlap and reduced carrier leakage leading to significantly improved threshold currents and performance at elevated temperatures. Furthermore, QDs provide broad gain for improved wavelength tunability and have low sensitivity to feedback. It should be noted that QD lasers have low modal gain and, as a result, typical laser cavity lengths are >1 mm.

The III-V laser epitaxial structure used for the development of micro-transfer printable QD laser coupons are grown by Innolume GmbH using molecular beam epitaxy (MBE) as shown in Fig. 3(a). The growth commences with a 500 nm thick $Al_{0.95}Ga_{0.05}As$ layer, which will act as the sacrificial release layer. This is followed by a 500 nm heavily doped GaAs n-contact layer, 1.35 μm n-type $Al_{0.3}Ga_{0.7}As$ lower cladding. The active region is composed of a stack of 14 InAs/GaAs QD layers lying within InGaAs layers. The epitaxial structure is completed with a 1.2 μm p-doped $Al_{0.4}Ga_{0.6}As$ upper cladding and a 50

nm heavily doped GaAs p-contact layer. The growth thicknesses are accurately controlled to enable vertical mode matching.

The definition of the laser devices starts with a Ti/Pt/Au p-metal deposition. Then, 2.5 μm wide ridge waveguides are formed with a 1.2 μm deep inductively coupled plasma (ICP) dry etch into the p-cladding layer using a 600 nm PECVD SiO_2 as hard mask. Smooth and vertical facets are defined by an ICP etch process using BCl_3-Cl_2-N_2-Ar chemistry together with the recess to the n-contact. For the devices reported here, the rear facet is formed with a multimode interference reflector (MIR) derived from a 1x2 multimode interference (MMI) coupler by terminating the output ports with two 45° deep etched mirrors [24]. The MMI reflector is 6.5 μm wide and 50 μm long. A scanning-electron microscope (SEM) image and schematic of the MMI mirror are given in Fig. 3(c). Light is imaged back onto the input waveguide by reflection from the etched mirror. The estimated obtained reflectivity is ~45%. The facets and coupon sidewalls are passivated by 240 nm PECVD SiN in order to protect the facets and the other epitaxial layers during subsequent fabrication steps and the release etch. A lift-off process is used to open the SiN mask and deposit an Au/Ge/Au/Ni/Au metal stack on the n-GaAs layer in the etched recess for the n-metal contact. Following opening of the dielectric on the p-contact, 40 nm/400 nm Ti/Au bond pads are deposited on the anode and cathode for electrical characterization. The resulting 65 μm wide etched-facet laser coupons are 1.5 mm, 1.8 mm and 2.4 mm long (corresponding laser cavity lengths are 1 mm, 1.5 mm and 2 mm, respectively) including the electrical top contact pads for probing the devices. A final ICP dry etch is required to remove the remaining n-type GaAs layer and define the coupon boundaries by etching 300 nm into the GaAs substrate using a resist mask. This process forms a 2 μm wide protrusion (ledge) from the facet. A schematic of the final laser is given in Fig. 3(b).

B. QD Laser Release

A 2.8 μm thick photoresist is used for the tethers that anchor the coupons to the source substrate during and after the release etch. The tethers are defined with an anti-phase arrangement [as shown in Fig. 4(a)]. This configuration is utilized to break the symmetric access of the release etchant to the sacrificial layer. The tether photoresist provides an extra encapsulation for the coupons while the openings between adjacent tethers allow the etchant to access the sacrificial layer. Then, the 500 nm thick $Al_{0.95}Ga_{0.05}As$ sacrificial layer is selectively removed in dilute hydrochloric acid solution [HCl (37%): H_2O = (1:1)] at 19 °C for 35 mins to release the laser coupons from the GaAs substrate. The average etch rate is ~1 μm/min with high selectivity to the surrounding GaAs. The formation of a thin oxide layer on the $Al_{0.95}Ga_{0.05}As$, due to the high Al content in sacrificial layer, requires a short (<45 sec) de-oxidation dip [Ammonium Hydroxide (25%): H_2O (1:10)] prior to release. The coupons are fully released with smooth surface on both the coupon stub [Fig. 4(b)] and bottom of the coupons [Fig. 4(c)]. A higher etch rate can be achieved by increasing the HCl concentration or by increasing the temperature of the solution. Doubling the HCl ratio leads a three-fold increase in the etch rate at 19 °C.

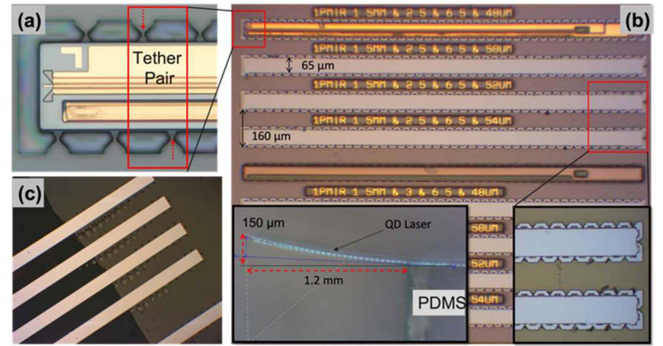

Fig. 4. (a) Photoresist tether defined with antiphase configuration on 65 μm wide coupon. (b) Microscope image of coupon stub on GaAs substrate after the pick-up. Side view of a laser coupon picked-up by bulk PDMS and curled due to stress on coupon (left-inset), Image of the coupon stubs shows a clean undercut (right-inset), (c) Image of bottom surface of coupons after the release etch.

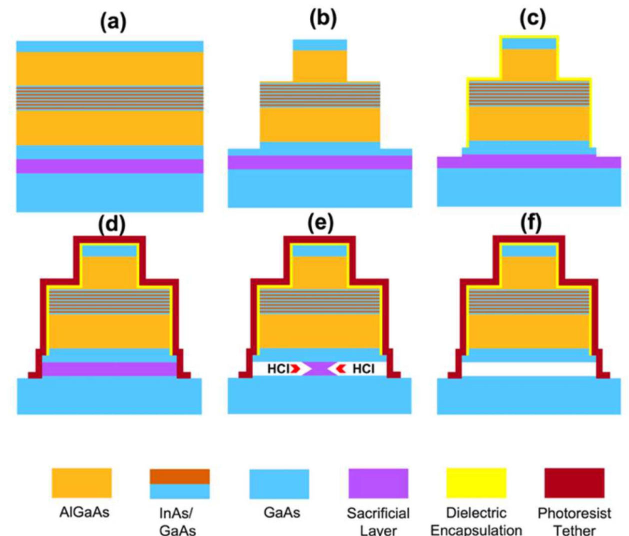

Fig. 5. Schematic fabrication process flow of MTP QD laser coupons on a GaAs substrate. (a) the initial epitaxial layer stack, (b) Device formation, (c) Second mesa formation and dielectric encapsulation, (d) Polymer (photoresist) anchor definition, (e) Undercut etch of sacrificial layer in HCl and (f) Fully released coupon anchored with tether.

Fig. 5 schematically shows the laser fabrication process flow and release etch steps.

The total stress on the laser coupons needs to be managed to achieve a high print yield during the transfer-print integration. This is particularly so for the QD laser coupons which, here, are up to 2.4 mm long with a width of 65 μm and thickness of < 5 μm. Any stress induced by the deposited dielectric and metal layers needs to be tailored by adjusting their net stress during the fabrication process to obtain essentially stress-free coupons. An example coupon (before optimization) picked-up by PDMS shows a slight tensile stress that leads the coupon to curve upwards by ~150 μm over a 1.2 mm distance as seen in Fig. 4(b)-left inset. Minimising the stress in the coupons improves the integration yield and reduces pillar formation during the release etch as discussed in [25].

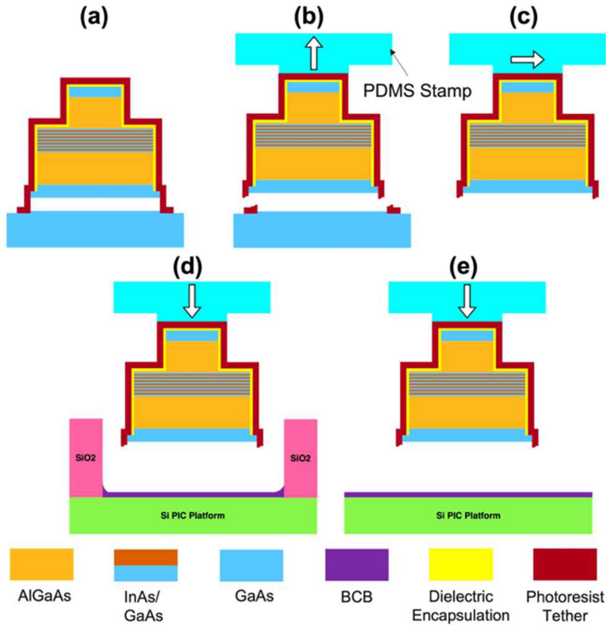

Fig. 6. Schematic sequence of picking and printing laser coupons onto target (a) Laser coupon ready for MTP, (b) Pick of the laser coupon with a PDMS stamp, (c) Transfer of coupon, (d) Integration into a recess on SOI or (e) Onto a planar surface.

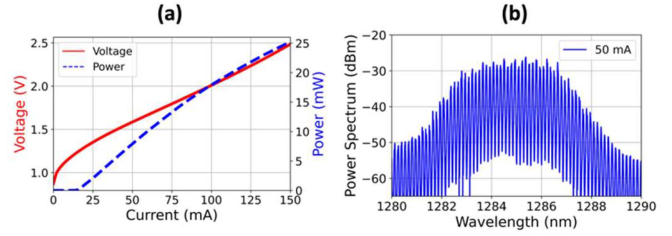

Fig. 7. (a) LIV curve of an etched-facet QD laser transferred on flat Si with 70 nm BCB at 20 °C. The 2.5 μm ridge laser with 1.5 mm cavity length has a threshold current of 17 mA with front facet output power of 17.5 mW at 100 mA bias current. (b) the laser spectrum (50 mA drive current, 20 °C) consists of multi-longitudinal modes with a 0.145 nm wavelength spacing.

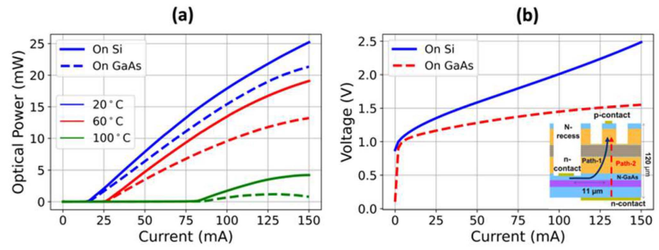

Fig. 8. (a) Temperature-dependent output power as a function of current for lasers with 2.5 μm-wide ridge and 1.5 mm cavity length on GaAs and after MTP ontp Si with 70 nm BCB, and (b) V-I characteristics of lasers on GaAs and Si at 20 °C. Electrical contact configuration and current path for lasers (inset).

IV. Edge Coupling to Waveguides

Following the release etch, QD laser coupons are integrated to SOI wafers using image recognition during MTP assisted by the fiducials on the laser and on the target. In this work, a single post polydimethylsiloxane (PDMS) stamp is used to pick-up and transfer the coupons onto the target chip as depicted in Fig. 6. This allows the lateral and longitudinal alignment to be typically ± 500 nm. The vertical alignment is set by the controlled epitaxial layer thicknesses and the corresponding waveguide layer thicknesses. Reference lasers are transfer-printed at the edge of an unstructured Si wafer with thin benzocyclobutene (BCB) (<70 nm) for laser characterization. In addition, lasers are printed into 7 μm deep recess with 100 nm spray-coated BCB, on 3 μm SOI and 300 nm SiN with 70 nm spin-coated BCB for edge-coupling measurements.

A. QD Laser Performance on Flat Si

Reference etched-facet lasers with the same ridge width and cavity lengths are fabricated in parallel with transfer-printable coupons. The electrical and spectral characterization of the lasers on the GaAs substrate and on the Si target wafer after MTP was conducted using a temperature-controlled stage. A Keithley 2600 source meter was used for biasing the devices through a pair of DC probes. The optical power was measured using a Newport 818IR Ge detector connected to a Newport 844-PE-USB power meter. The lasers on GaAs and Silicon are characterized under continuous-wave (CW) current condition. Transfer-printed QD lasers with 1.5 mm cavity shows a lasing threshold current of 17 mA and output power of 17.5 mW under 100 mA injection current at 20 °C as shown in Fig. 7(a). Spectral characterization was conducted using an ANDO AQ6317B optical spectrum analyzer (OSA) with a resolution bandwidth of 0.01 nm. Fig. 7(b) shows the multi-longitudinal mode lasing spectrum of the laser emitting around 1285 nm. The spectrum consists of the cavity Fabry–Perot modes with a wavelength spacing ($\Delta\lambda$) of 0.145 nm which corresponds to a group index of ∼3.41 and cavity length of 1.5 mm in agreement with the theoretical values.

Fig. 8(a) shows the measured optical power as a function of drive current for various operating temperatures up to 100 °C and compares the MTP laser coupon with an identical device configuration on the source GaAs wafer. Both lasers have similar threshold currents with different thermal rollover characteristics. At 100 °C, the threshold current rises to 85 mA and the slope efficiency decreases from 0.21 W/A (at 20 °C) to 0.025 W/A. Although the laser is transferred on a 70 nm thick BCB layer that reduces heat extraction, temperature-dependent light-current (L-I) characteristics shows an improved thermal performance compared to the laser on GaAs due to the superior thermal conductivity of Si (1.3 W /cm. °C) over GaAs (0.52 W /cm. °C). Similar improved thermal characteristics were reported in [26] for InP lasers transfer-printed directly on Si with no adhesive layer.

The voltage-current (V-I) characteristics for lasers on GaAs and transferred on Si are given in Fig. 8(b) where differential series resistances of 4.5 Ω and 8.7 Ω are measured, respectively. Both lasers have a top p-contact but whereas the MTP device has its n-contact on the top side on a recessed area etched to the n^+-GaAs layer as depicted in the inset of Fig. 8(b), the reference laser on GaAs has its n-contact deposited on the substrate that

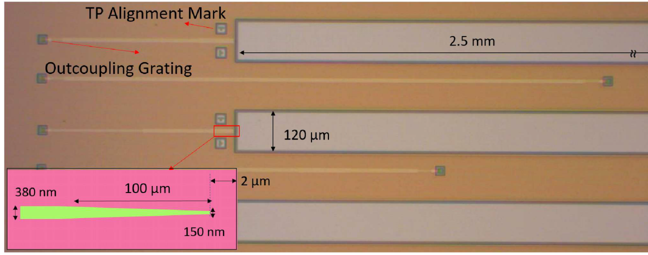

Fig. 9. Plane view optical microscope image of the 7 μm deep, 120 μm wide and 2.5 mm long recesses defined in SOI. The inset shows the schematic of single tip Si waveguide inverse tapered from 150 nm to 380 nm over a 100 μm distance. Waveguide tip is recessed from the etched facet by 2 μm.

results in it having a lower series resistance. The electron current is required to flow laterally over the remaining 350 nm thick n-GaAs on the transferred laser leading to the increased resistance.

B. QD Laser Performance on 220 Nm SOI

The 120 μm wide and 2.5 mm long recesses that adjoin the submicron sized receiving Si waveguides with a single tip are fabricated on the 220 nm SOI platform with 300 mm diameter wafers at imec (iSiPP50G short loop). The chips include surface out-coupling gratings and alignment marks for MTP as seen in Fig. 9. The Si waveguide is tapered from 150 nm to 380 nm over a 100 μm distance as schematically shown in the inset of Fig. 9. The tip is recessed from the etched facet by a nominal 2 μm.

A 100 nm thick BCB, spray-coated by EV Group, is utilized as an adhesive interlayer to achieve high print yield. QD laser coupons up to 2.4 mm long are transfer-printed with a high yield ($>$ 95%) into the 7 μm deep recess on the SOI wafer. Following the tether removal in O_2 plasma, the BCB bonding layer is fully cured at 250 °C. Fig. 10(a) shows a microscope image of QD laser coupons with different lengths integrated into the recesses on the SOI wafer. Although an alignment accuracy of $<$ 0.5 μm is achievable with MTP, the longitudinal misalignment in the transferred coupons is measured 7 μm as can be seen in the SEM image in Fig. 10(b). Including the 2 μm recess of the Si taper tip within the SOI, the total gap in the longitudinal direction is 9 μm. In addition to the 2 μm wide ledge defined for the encapsulation around the coupon, the BCB piling on trench edge during spray-coating process prevents the laser to be printed closer than 5 μm. In this situation, the printing of the laser closer would result in the laser to be tilted upwards deteriorating the coupling. The lateral misalignment of the laser facet to the Si waveguide is measured to be $<$ 0.5 μm [as given in Fig. 10(c)] using image-recognition during MTP that utilizes the alignment markers on both SOI target and laser. Vertical alignment is achieved by adjusting the etch depth of the recess on the SOI wafer and the adhesive interlayer thickness. A Focused Ion Beam (FIB) cross section of the SOI waveguide [Fig. 10(d)] indicates a vertical misalignment of $<$ 200 nm caused by the variation in the material and adhesive thickness.

Electrical and optical measurements of the integrated laser diodes is conducted in CW mode at room temperature. Waveguide coupled power is collected using a 10° tilted flat cleaved

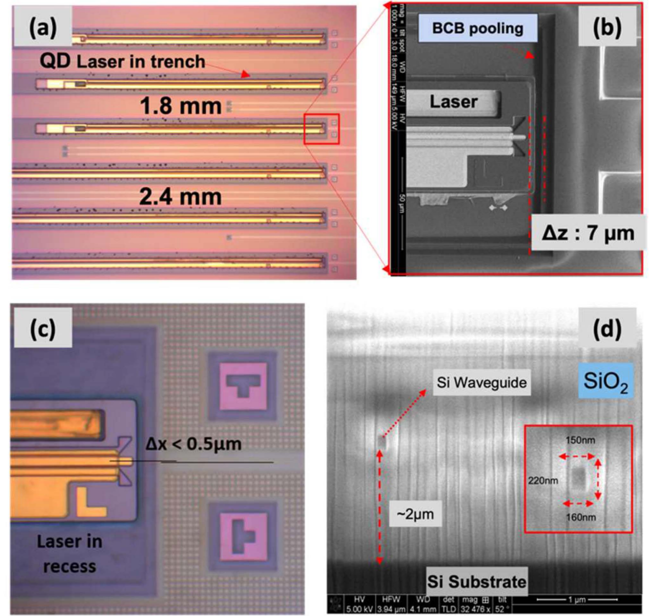

Fig. 10. (a) Images of 1.8 mm and 2.4 mm long QD laser coupons MTP into 7 μm deep trenches on SOI with 100 nm spray-coated BCB. (b) SEM image of a coupon inside deep trench shows 7 μm longitudinal spacing between laser and SOI facet due to BCB pooling at recess edge. (c) Detail of the lasing facet shows a lateral misalignment of $\Delta x < 0.5$ μm. (d) FIB cross section image near the Si waveguide tip shows the Si waveguide is 150 nm wide and 220 nm thick.

single mode fiber via the surface grating coupler as schematically shown in Fig. 11(a). The light-current (L-I) characterization is conducted after the longitudinal spacing between laser and waveguide is in-filled with a refractive index matching polymer (Norland 61 UV sensitive fiber glue with refractive index of 1.56) followed by 4 mins cure under 365 nm LED. Up to 250 μW light is measured in the receiving single mode fiber [as shown in Fig. 11(b)] as reported in [21]. The 1.8 mm long device shows a threshold current, I_{th}, of 19 mA and ∼25 mA before and after the in-fill, respectively, as given in Fig. 11(c). The slight rise in the threshold current is due to the polymer which reduces the facet reflectivity.

Using reference waveguides with in and out-coupling gratings, the best coupling from grating to fiber is measured to be -6 dB, and so a minimum internal waveguide power of 1 mW is estimated at 85 mA drive current. Considering the amount of power that the laser is producing, the amount of waveguide coupled light suffers from misalignments. The longitudinal misalignment of $>$ 7 μm as measured in the SEM image in Fig. 10(b) is the main source of the loss. However, the gap between the laser and SOI facet can be reduced by the removal of BCB pooling and the ledge on the laser coupon. Simulation results shown in Fig. 2 predict a near 10-fold increase in coupling with optimum positioning of the laser.

C. QD Laser Performance on 3 µm SOI

1.5 mm long coupons (1 mm long laser cavity) are integrated on a 3 μm SOI waveguide wafer with high yield ($>$ 95%) by MTP in manual mode without using pattern recognition. Laser

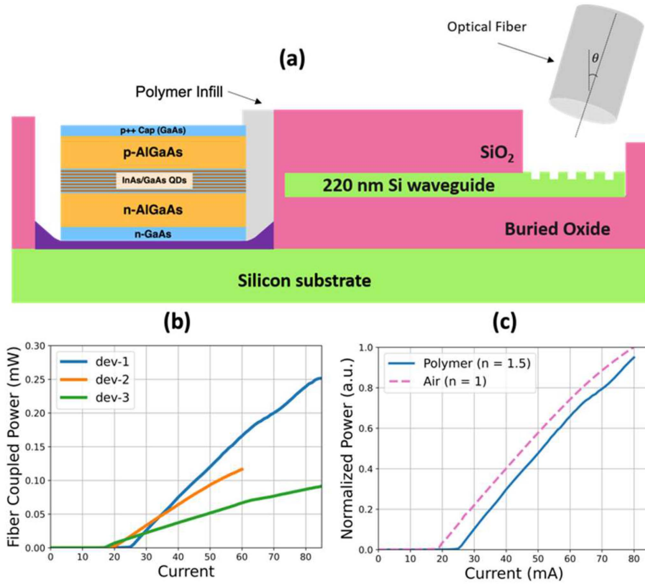

Fig. 11. (a) Schematic of coupling from a laser printed in SOI trench to 220 nm Si waveguide and then to single mode fiber through the out-coupling grating. (b) Fiber coupled power as a function of current for 3 devices. (c) L-I curve (for dev-1) shows the change in threshold current before and after the longitudinal gap is filled with an index matching polymer. The light intensity is normalized for better comparison.

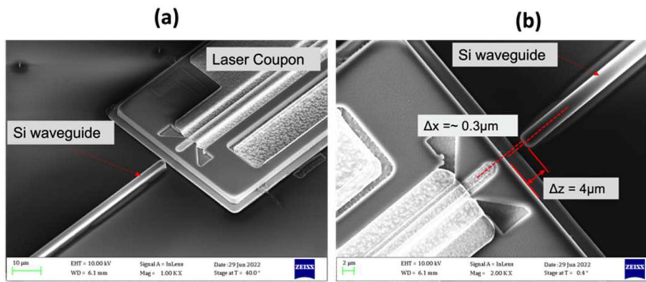

Fig. 12. (a) SEM image of a 1.5 mm long QD laser coupon placed in front of a 3 μm thick, deep-etched waveguide on SOI wafer. (b) Lateral and longitudinal alignment of laser with respect to the Si waveguide.

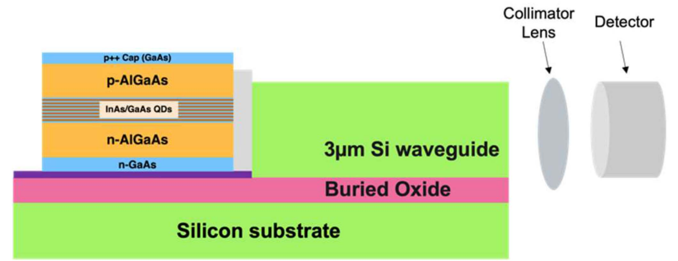

Fig. 13. Schematic of edge-coupling from a laser to 3 μm thick Si waveguide and the coupling from the cleaved facet to a broad area detector.

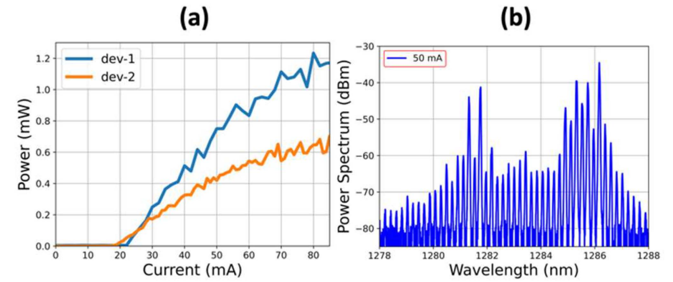

Fig. 14. (a) L-I characteristics measured with a broad area detector emerging from the 3 μm thick waveguide. (b) the emission spectrum of the waveguide coupled light at 20 °C with 50 mA drive current.

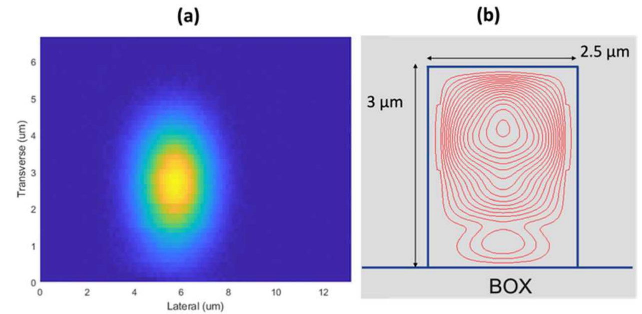

Fig. 15. (a) Measured near field beam profile at the exit of the 5 mm long Si waveguide. (b) Simulated electric field of the excited mode in 2.5 μm wide and 3 μm thick Si waveguide when the vertical misalignment between laser and receiving waveguide is 0.67 μm.

coupons are transferred directly on the 1 μm BOX layer after 70 nm BCB is spin coated on the target as the adhesion layer. A SEM image of a QD laser coupon printed next to a 3 μm thick and 2.5 μm wide waveguide is shown in Fig. 12(a). The lateral and longitudinal alignment of the laser to the Si waveguide is measured to be $\Delta x = 0.3$ μm and $\Delta z = 4$ μm, respectively as shown in Fig. 12(b). Positional alignment in both directions can be enhanced using the image-assisted printing. The vertical alignment between the laser and waveguide can be controlled by the etch depth into the SOI and adhesive thickness. Here, the mismatch in the vertical direction is calculated to be 0.67 μm due to the difference between the mode center in the laser (2.1 μm +0.07 μm BCB) and Si waveguide (1.5 μm).

The waveguide coupled light is collected using a lens-ended single mode fiber with 3 μm spot size as shown in Fig. 13. The LI curves show that the best laser has an I_{th} of 21 mA with an output power up to 1.2 mW at 85 mA, as shown in Fig. 14(a). The internal waveguide power is above 1.7 mW given the exit facet has a reflectivity of $\sim$30%. The longitudinal spacing between laser and Si waveguide facet is filled by a glue with refractive index of 1.56, which results in an increase of I_{th} by 4 mA. Fig. 14(b) shows the measured multi-mode lasing spectrum of the laser at 50 mA. The laser emits around 1284 nm wavelength. The wavelength spacing of 0.145 nm indicates that the modes belong to the laser with 1 mm Fabry-Perot cavity.

Fig. 15(a) presents a near-field image of the 3 μm Si waveguide taken while the laser is biased at 50 mA. The 2D scan is recorded by scanning the single mode lensed fiber across the waveguide in lateral and vertical direction using Elliot Scientific DALi 2100 3-Axis piezo auto-aligning controller. Optimized vertical alignment is necessary in order to minimize the coupling into higher order modes. Fig. 15(b) illustrates the electric field

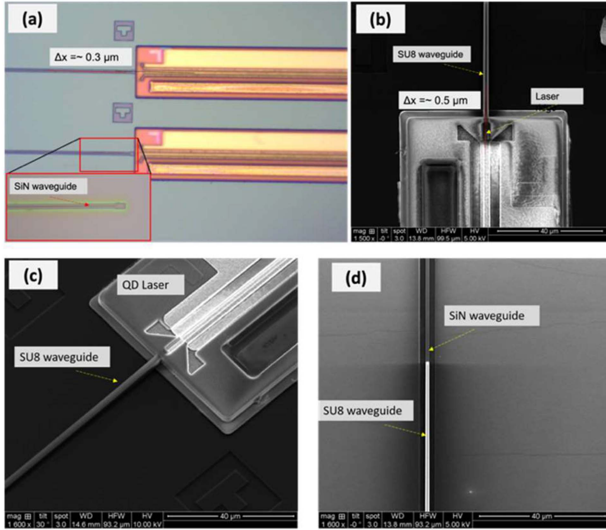

Fig. 16. (a) 1.8 mm long QD laser coupon transfer-printed on 70 nm BCB. The inset shows the SiN waveguide that starts from ∼10 μm away from the laser facet. (b) SEM image of a laser after SU-8 polymer waveguide definition. (c) Side view of a laser shows there is no gap between the laser facet and receiving SU-8 polymer waveguide. (d) SEM image of 1 μm wide SiN waveguide and SU-8 waveguide termination tip.

(E_x) of the excited mode in the Si waveguide when the light is coupled with a 0.67 μm misalignment in the vertical direction into the receiving waveguide.

D. QD Laser Performance on SiN Waveguide Platform

1.8 mm long QD laser coupons (1.5 mm cavity length) are heterogeneously integrated to a SiN waveguide platform. 1 μm wide SiN waveguides are defined by e-beam lithography and etching. 70 nm BCB is spin coated and QD laser coupons are successfully printed as shown in Fig. 16(a). After tether resist removal in O_2 plasma and BCB cure at 250 °C, a 2.2 μm thick spin-coated SU-8 polymer waveguide is patterned using an e-beam process. The lateral misalignment of the laser ridge with respect to the SiN waveguide and SU-8 polymer waveguide is measured as $\Delta x = \sim 0.3$ μm [as given in Fig. 16(a)] and $\Delta x = \sim 0.5$ μm [as given in Fig. 16(b)], respectively. The vertical alignment between the laser and SU-8 waveguide can be controlled by the etch depth into BOX layer and adhesive thickness or SU-8 thickness. Here, the mismatch in the vertical direction is ∼ 0.7 μm. There is no longitudinal spacing between the emitting facet and SiN waveguide as the SU-8 polymer waveguide starts from the laser facet as seen in Fig. 16(c).

The 300 nm thick SiN waveguide is inverse-tapered from 100 nm to 1 μm over a 200 μm distance while the SU-8 polymer waveguide is tapered from 3 μm to 500 nm to enable the evanescent coupling as shown in Fig. 17(a). The chip is cleaved 4 mm away from the laser and output light is collected by a broad area detector with a collimating lens as schematically shown in Fig. 17(b). The measurements are carried out at 20 °C under CW operation.

The LI curve shows that the laser with 1.5 mm long cavity has an I_{th} of 26 mA and 0.85 mW waveguide-emitted power at 85 mA as seen in Fig. 18(a). The estimated internal waveguide power is 0.95 mW. The interface of the laser with SU-8 (n ∼ 1.6) results in a similar threshold current increase as before. The laser emission at 50 mA is captured using an IR camera in Fig. 18(b). The bright spot indicates the light is coming out from the cleaved end of the 4 mm long SiN waveguide. Two other bright spots are seen in the image corresponding to the rear facet and the laser – SU-8 interface. Loss in the waveguide due to substrate coupling can also be discerned. In addition to optimisation of the alignment, improving the mirror reflectivity and engineering the SU-8 polymer waveguide dimensions, will reduce these losses, and enable the realization of other types of lasers [27].

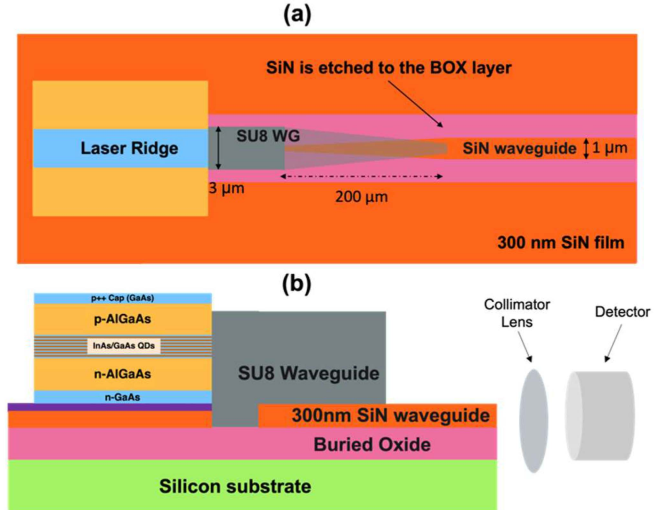

Fig. 17. (a) Top view of the platform including integrated QD laser, SU-8 and SiN waveguide arrangement. (b) Light coupling schematic from laser to SU-8 polymer waveguide and SiN waveguide. Light from the cleaved end of 4 mm long SiN waveguide is collected by a broad area detector using a collimating lens.

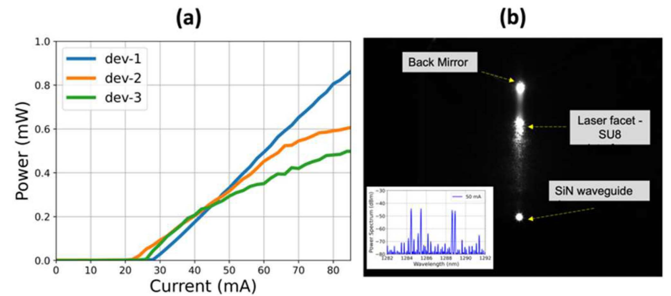

Fig. 18 (a) Measured L-I characteristics from 1.5 mm long laser coupons integrated with a SiN waveguide. Signal is first edge-coupled into 3 μm wide and 2.2 μm thick SU-8 waveguide, and then evanescently coupled to underlying SiN waveguide. The inset shows the spectrum of waveguide coupled light at 20 °C. (b) Infra-red camera plan view image of the laser and SiN when the laser is biased at 50 mA.

The simulated and measured coupling performance for each platform is compared considering the estimated power delivered by the reference laser at the same bias current (85 mA). The simulated coupling efficiencies after including the losses due to positioning misalignment are 13%, 15% and 12% for 220 nm

SOI, 3 μm SOI and 300 nm SiN platforms, respectively while the measured corresponding coupling efficiencies are 7.5%, 12% and 7%. Although there is a slight difference between simulation and measurement, the measured efficiencies can be considered reasonable including other potential loss mechanisms (i.e., variation in laser performance, waveguide loss, substrate coupling and higher order mode coupling loss).

V. Conclusion

Integrated edge-coupling of light to waveguides via MTP of components is a versatile solution to enhancing the functionality and applicability of emerging PICs. QD lasers can be fabricated in a III-V fabrication facility while the Si PICs can be realized in open-access CMOS foundries enabling the heterogeneous integration of optimized devices using MTP. Vertical control can be engineered during the fabrication and MTP offers positional control to sub-micron dimensions. High transfer printing yield (>90%) is obtained for narrow coupons up to 2.4 mm in length by using an ultra-thin BCB adhesive. The performance of the lasers is not compromised by the transfer printing process and the thermal performance is improved when integrating the III-V lasers on Si. When placed on a thick BOX layer the thermal rollover is evident. The coupling efficiency is dependent on positional control and filling of the gap. Adjustments in the chip design (reducing ledge), improving the etched facet quality and in the BCB process (removing pooling) are straightforward ways to advance the performance.

We have demonstrated the versatility of the technology with the same lasers integrated with different waveguide platforms. Similarly, other devices (photodetectors modulators) could be integrated with an edge-coupled configuration. Each design could be adapted for any specific device.

Acknowledgment

The authors would like to acknowledge the Tyndall fabrication facility, Alan Blake for assistance related to processing of 3 μm SOI and Simone Varo for assisting with the fiber glue application.

References

[1] D. Thomson et al., "Roadmap on silicon photonics," *J. Opt.*, vol. 18, no. 7, 2016, Art. no. 073003.

[2] D. Pérez et al., "Multipurpose silicon photonics signal processor core," *Nature Commun.*, vol. 8, 2017, Art. no. 636.

[3] M. A. Nahmias et al., "Photonic multiply-accumulate operations for neural networks," *IEEE J. Sel. Topics Quantum Electron.*, vol. 26, no. 1, Jan./Feb. 2020, Art. no. 7701518.

[4] S. Porto et al., "Demonstration of a 2× 800 Gb/s/wave coherent optical engine based on an InP monolithic PIC," *J. Lightw. Technol.*, vol. 40, no. 3, pp. 664–671, 2022.

[5] M. C. Tien, J. F. Bauters, M. J. R. Heck, D. J. Blumenthal, and J. E. Bowers, "Ultra-low loss Si_3N_4 waveguides with low nonlinearity and high power handling capability," *Opt. Exp.*, vol. 18, pp. 23562–23568, 2010.

[6] M. Zhang et al., "Broadband electro-optic frequency comb generation in a lithium niobate microring resonator," *Nature*, vol. 568, pp. 373–377, 2019.

[7] R. Zhao et al., "Hybrid dual-gain tunable integrated InP-Si3N4 external cavity laser," *Opt. Exp.*, vol. 29, pp. 10958–10966, 2021.

[8] T. Barwicz et al., "A novel approach to photonic packaging leveraging existing high-throughput microelectronic facilities," *IEEE J. Sel. Topics Quantum Electron.*, vol. 22, no. 6, Nov./Dec. 2016, Art. no. 8200712.

[9] A. W. Fang et al., "Electrically pumped hybrid AlGaInAs-silicon evanescent laser," *Opt. Exp.*, vol. 14, pp. 9203–9210, 2006.

[10] M. A. Meitl et al., "Transfer printing by kinetic control of adhesion to an elastomeric stamp," *Nature Mater.*, vol. 5, no. 1, pp. 33–38, 2006.

[11] A. Carlson, A. M. Bowen, Y. Huang, R. G. Nuzzo, and J. Rogers, "Transfer printing techniques for materials assembly and micro/nanodevice fabrication," *Adv. Mater.*, vol. 24, pp. 5284–5318, 2012.

[12] J. Justice et al., "Wafer-scale integration of group III–V lasers on silicon using transfer printing of epitaxial layers," *Nature Photon.*, vol. 6, pp. 610–614, 2012.

[13] C. O. d. Beeck et al., "Heterogeneous III-V on silicon nitride amplifiers and lasers via microtransfer printing," *Optica*, vol. 7, pp. 386–393, 2020.

[14] B. Haq et al., "Micro-transfer-printed III-V-on-silicon C-band distributed feedback lasers," *Opt. Exp.*, vol. 28, pp. 32793–32801, 2020.

[15] R. Katsumi, O. Y. Ota, T. Yamaguchi, and Y. Arakawa, "Quantum-dot single-photon source on a CMOS silicon photonic chip integrated using transfer printing," *APL Photon.*, vol. 4, no. 3, 2019, Art. no. 036105.

[16] B. Guilhabert et al., "Hybrid integration of an evanescently coupled AlGaAs microdisk resonator with a silicon waveguide by nanoscale-accuracy transfer printing," *Opt. Lett.*, vol. 43, no. 20, pp. 4883–4886, 2018.

[17] J. Juvert et al., "Integration of etched facet, electrically pumped, C-band Fabry-Pérot lasers on a silicon photonic integrated circuit by transfer printing," *Opt. Exp.*, vol. 26, pp. 21443–21454, 2018.

[18] R. Loi et al., "Edge-coupling of O-band InP etched-facet lasers to polymer waveguides on SOI by micro-transfer-printing," *IEEE J. Quantum Electron.*, vol. 56, no. 1, Feb. 2020, Art. no. 6400108.

[19] J. Goyvaerts et al., "Transfer-print integration of GaAs pin photodiodes onto silicon nitride waveguides for near-infrared applications," *Opt. Exp.*, vol. 28, no. 14, pp. 21275–21285, 2020.

[20] Y. Wang et al., "Responsibility optimization of a high-speed InP/InGaAs photodetector with a back reflector structure," *Opt. Exp.*, vol. 30, pp. 4919–4929, 2022.

[21] A. Uzun et al., "Integration of quantum dot lasers with SOI waveguides using micro transfer printing," in *Proc. Italy-23rd Eur. Conf. Integr. Opt.*, 2022, pp. 1–3.

[22] A. Bera, Y. Marin, M. Harjanne, M. Cherchi, and T. Aalto, "Ultra-low loss waveguide platform in silicon photonics," *Proc. SPIE*, vol. 12006, 2022, pp. 6–11.

[23] G. Roelkens, D. Van Thourhout, R. Baets, R. Nötzel, and M. Smit, "Laser emission and photodetection in an InP/InGaAsP layer integrated on and coupled to a silicon-on-insulator waveguide circuit," *Opt. Exp.*, vol. 14, pp. 8154–8159, 2006.

[24] E. Kleijn, M. K. Smit, and X. J. M. Leijtens, "Multimode interference reflectors: A new class of components for photonic integrated circuits," *J. Lightw. Technol.*, vol. 31, no. 18, pp. 3055–3063, Sep. 2013.

[25] B. Corbett, R. Loi, J. O'Callaghan, and G. Roelkens, "Transfer printing for silicon photonics," in *Semiconductors and Semimetals*. New York, NY, USA: Elsevier, 2018, pp. 43–70.

[26] R. Loi et al., "Thermal analysis of InP lasers transfer printed to silicon photonics substrates," *J. Lightw. Tech.*, vol. 36, no. 24, pp. 5935–5941, Dec. 2018.

[27] A. P. Bakoz et al., "Wavelength stability in a hybrid photonic crystal laser through controlled nonlinear absorptive heating in the reflector," *Light: Sci. Appl.*, vol. 7, no. 39, 2018, Art. no. 39.

Ali Uzun received the B.Sc. degree in computer science and electrical and electrotonic engineering, and the M.Sc. degree in electronics and computer engineering from Istanbul Sehir University, Istanbul, Turkey, in 2016 and 2019, respectively. He is currently working toward the Ph.D. degree in electrical engineering with Tyndall National Institute, University College Cork, Cork, Ireland. He is currently working on the European project CALADAN. His research interests include design and fabrication of III-V materials and devices and their integration onto Silicon photonics platforms by micro transfer printing.

Fatih Bilge Atar received the B.Sc. and Ph.D. degrees in electrical and electronics engineering from Bilkent University, Ankara, Turkey. He is currently a Postdoctoral Researcher with the III–V Materials and Devices Group, Tyndall National Institute, Cork, Ireland. His research interests include optoelectronic devices, heterogeneous integration of III-V materials with Si photonics, and photonic integrated circuit design.

Simone Iadanza was born in Tradate, (Varese), Italy, in 1989. He received the B.Sc. degree in engineering physics and the M.Sc. degree in materials engineering and nanotechnology from the Politecnico di Milano, Milan, Italy, in 2012 and 2016, respectively, and the Ph.D. degree in physics with Munster Technological University, Cork, Ireland, in 2022. He is currently working on the European DANCeR and RedFinch projects. His research interests include nano-photonics, opto-electronics and nanofabrication of photonic crystals, silicon photonics, and semiconductor lasers dynamics.

Ruggero Loi was born in Cagliari, Italy, in 1980. In 2013, he received the M.Sc. degree in applied physics with the University of Cagliari, Cagliari, Italy, the Ph.D. degrees in engineering science – photonics with Irish Photonic Integration Centre, Tyndall National Institute, University College Cork, Cork, Ireland, in 2019. He pioneered the heterogeneous integration of III-V devices onto different platforms by μTP since 2014 and has authored several scientific publications and a few patents in the field of integrated photonics. He was involved in the EU project TOP-HIT and he is actively contributing to the EU projects CALADAN and INSPIRE.

Jing Zhang received the B.Sc. degree in physics and the M.Sc. degree in optics from Northwest University, Xi'an, China, in 2009 and 2012, respectively, and the Ph.D. degree in photonics with the Photonics Research Group, Department of Information Technology, Ghent University–IMEC, Ghent, Belgium. His research interests include heterogeneous integration of III–V on Si devices, tunable and narrow linewidth laser, integrated coherent receiver, and transfer printing integration of III–V optoelectronic components.

Gunther Roelkens (Senior Member, IEEE) received the degree in electrical engineering from Ghent University, Belgium, in 2002, and the Ph.D. degree from Department of Information Technology, Ghent University, in 2007. He is currently a Full Professor with Ghent University. In 2008, he was a Visiting Scientist with IBM TJ Watson Research Center, New York. His research interests include the heterogeneous integration of III-V semiconductors and other materials on top of silicon waveguide circuits and electronic/photonic co-integration. He was holder of an ERC starting grant (MIRACLE), to start up research in the field of integrated mid-infrared photonic integrated circuits.

Igor Krestnikov received the Ph.D. degree from Ioffe Physico-Technical Institute, St.Petersburg, Russia, in 1998, doing his Ph.D. research work with the Group of nobel laurate Professor Zhores Alferov. In 2003, he joined Innolume to lead several customer-based projects. He is currently focuses on development and fabrication of quantum dot devices for communication solutions in a position of Production Manager. Prior to Innolume, Dr. Krestnikov spent three years with the Technical University of Berlin, Berlin, Germany, as a Research Fellow.

Johanna Rimböck was born in Vilshofen, Germany, in 1981. She received the graduation degree in biotechnological engineering from the University of Applied Sciences Weihenstephan, Freising, Germany, in 2006. She is the Head of process technology for coaters and developers with EV Group headquarters, St. Florian, Austria. Her current work covers all areas of lithography, especially different coating technologies for various applications.

Liam O'Faolain (Member, IEEE) was born in Cork, Ireland. He received the Ph.D. degree from the University of St. Andrews, St. Andrews, Scotland. In 2012, he joined the Group of Prof. David A. B. Miller, Stanford University, Stanford, CA, USA, as an SU2P Entrepreneurial Fellow before returning to take up a lecturing position at St Andrews in 2013. In 2016, he re-located his research group to the Centre for Advanced Photonics and Process Analysis, Munster Technological University, Cork, Ireland. He is one of the leading authorities on disorder and loss in photonic crystal waveguides and has designed and realized the world's best slow light waveguides to date. He has authored or coauthored more than 100 journal articles. His research group works on a range of projects using nano-photonics, hybrid lasers and integrated optics for applications in optical communications and optical sensing.

Brian Corbett received the B.Sc. degree in experimental physics and mathematics and the M.Sc. degree from Trinity College, Dublin, Ireland. He is currently the Head of the III–V Materials and Devices Group, Tyndall National Institute and principal investigator in the Irish Photonics Integration Centre (IPIC). He has been engaged in developing III–V micromachining expertise using dry and wet-etching techniques. This technology has been applied in low-cost single-frequency lasers, micro-LEDs and photodetectors. His main research focuses on photonic integrated circuits.